Supporting Information

Wylie et al. 10.1073/pnas.1319577110

SI Text

Chemical Shift Analysis. This hypothesis that the low potassium state exhibits opening of the inner transmembrane helices was further explored using available structures of open or semi open channels, via chemical shift prediction tools. Recent structural models of truncated KcsA with the pH gate open (Protein Data Bank ID codes 3FB8 and 3F5W) are depicted in Fig. S4, showing a very distinct helical kink near residue F103. To test the hypothesis that evacuation of K^+ from the selectivity filter shifts the protein toward a variation of the open, inactivated structure, we chose to compare our experimentally determined chemical shifts against chemical shifts back-predicted from known crystal structures. After hydrogens were added to these structures in MolProbity (1–8), the chemical shifts were predicted using the SPARTA+ (9, 10). Results for the chemical shift prediction are provided in Table S2. We focused on the ^{13} Cα chemical shifts, which are known to be the strongest indicators of backbone dihedral conformation and exhibit the best chemical shift prediction accuracy (9, 11). In this analysis, we included a low K^+ structure (1K4D) (12) and a series of structures with different degrees of opening, measured at T112 and ranging from 14 Å (3FB5) to 32 Å (3F5W) (13–18). It is expected and even well known that the accuracy of chemical shift prediction degrades with decreasing structural resolution accuracy, and also that prediction accuracy further degrades in poorly populated regions of Ramachandran space such as the selectivity filter (9, 11). In keeping with this consideration, the chemical shifts predicted using the 1K4D crystal structure are generally in better agreement with the experiment than are the predictions from other lower resolution structures [like the 1K4D structure, these mutants were prepared with both *N*- and C-terminal deletions and are also septuple mutants of KcsA (H25Q, L90C, R117Q, E120Q, R121Q, R122Q, and H124Q)]. However, in the hinge region the trend is different. Overall, the best agreements between prediction and experiment for the hinge residues are achieved for structures 3F7Y and 3FB8. These structures exhibit altered kinks with intermediate openings of 17 Å and 20 Å, respectively (measured at T112). This tentatively suggests a modest helical kink in the inner transmembrane helix, consistent with the structure pictured in green in Fig. S4. It has been suggested that an opening of about 20 Å is required to cause appearance of the collapsed state of the selectivity filter, for example when at low pH opening precedes inactivation. Possibly active removal of the ion induces a global conformational change and opening to a similar extent.

1. Baldus M, Petkova AT, Herzfeld J, Griffin RG (1998) Cross polarization in the tilted frame: Assignment and spectral simplification in heteronuclear spin systems. *Mol Phys* 95(6):1197–1207.
2. Fung BM, Khitrin AK, Ermolaev K (2000) An improved broadband decoupling sequence for liquid crystals and solids. *J Magn Reson* 142(1):97–101.
3. Takegoshi K, Nakamura S, Terao T (2003) C-13-H-1 dipolar-driven C-13-C-13 recoupling without C-13 rf irradiation in nuclear magnetic resonance of rotating solids. *J Chem Phys* 118:2325–2341.
4. Hing AW, Vega S, Schaefer J (1992) Transferred-echo double-resonance NMR. *J Magn Reson* 96:205–209.
5. Franks WT, Kloepper KD, Wylie BJ, Rienstra CM (2007) Four-dimensional heteronuclear correlation experiments for chemical shift assignment of solid proteins. *J Biomol NMR* 39(2):107–131.
6. Costa PR, Sun BQ, Griffin RG (1997) Rotational resonance tickling: Accurate internuclear distance measurement in solids. *J Am Chem Soc* 119:10821–10830.
7. Chen VB, et al. (2010) MolProbity: All-atom structure validation for macromolecular crystallography. *Acta Crystallogr D Biol Crystallogr* 66(Pt 1):12–21.
8. Davis IW, et al. (2007) MolProbity: All-atom contacts and structure validation for proteins and nucleic acids. *Nucleic Acids Res* 35(Web Server issue):W375–W383.
9. Shen Y, Bax A (2007) Protein backbone chemical shifts predicted from searching a database for torsion angle and sequence homology. *J Biomol NMR* 38(4):289–302.
10. Shen Y, Bax A (2010) SPARTA+: A modest improvement in empirical NMR chemical shift prediction by means of an artificial neural network. *J Biomol NMR* 48(1):13–22.
11. Neal S, Nip AM, Zhang HY, Wishart DS (2003) Rapid and accurate calculation of protein 1H, 13C and 15N chemical shifts. *J Biomol NMR* 26(3):215–240.
12. Zhou YF, Morais-Cabral JH, Kaufman A, MacKinnon R (2001) Chemistry of ion coordination and hydration revealed by a K+ channel-Fab complex at 2.0 A resolution. *Nature* 414(6859):43–48.
13. Cuello LG, Jogini V, Cortes DM, Perozo E (2010) Structural mechanism of C-type inactivation in K(+) channels. *Nature* 466(7303):203–208.
14. Cordero-Morales JF, et al. (2006) Molecular determinants of gating at the potassium-channel selectivity filter. *Nat Struct Mol Biol* 13(4):311–318.
15. Cordero-Morales JF, Jogini V, Chakrapani S, Perozo E (2011) A multipoint hydrogen-bond network underlying KcsA C-type inactivation. *Biophys J* 100(10):2387–2393.
16. Cordero-Morales JF, et al. (2007) Molecular driving forces determining potassium channel slow inactivation. *Nat Struct Mol Biol* 14(11):1062–1069.
17. Lockless SW, Zhou M, MacKinnon R (2007) Structural and thermodynamic properties of selective ion binding in a K+ channel. *PLoS Biol* 5(5):e121.
18. Cuello LG, et al. (2010) Structural basis for the coupling between activation and inactivation gates in K(+) channels. *Nature* 466(7303):272–275.

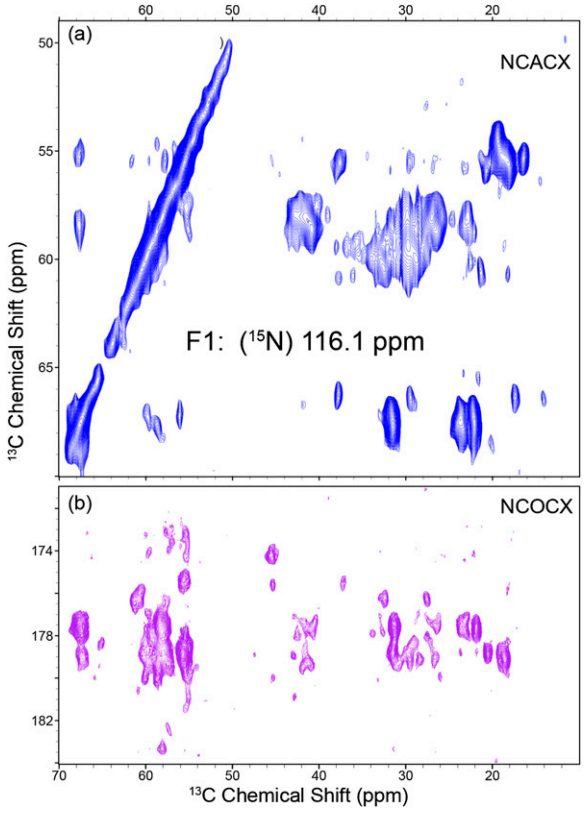

Fig. S1. 2D planes from 3D NCC spectra. Displayed are planes from NCACX (*N*-Cα-$C_{i,sidechain}$) (blue, *A*) and NCOCX (*N*-C′-$C_{i-1,sidechain}$) (purple, *B*) spectra. Both planes correspond to a common ^{15}N chemical shift of 116.1 ppm. Although line-widths are relatively good for a membrane protein, like in Figs. 4 and 5, the spectral overlap is still significant. Although there are several well-resolved outliers in these spectra, overall most resonances are overlapped. Although most regions of the spectra can be assigned to specific residue types, assignment of many regions of these spectra are completely ambiguous.

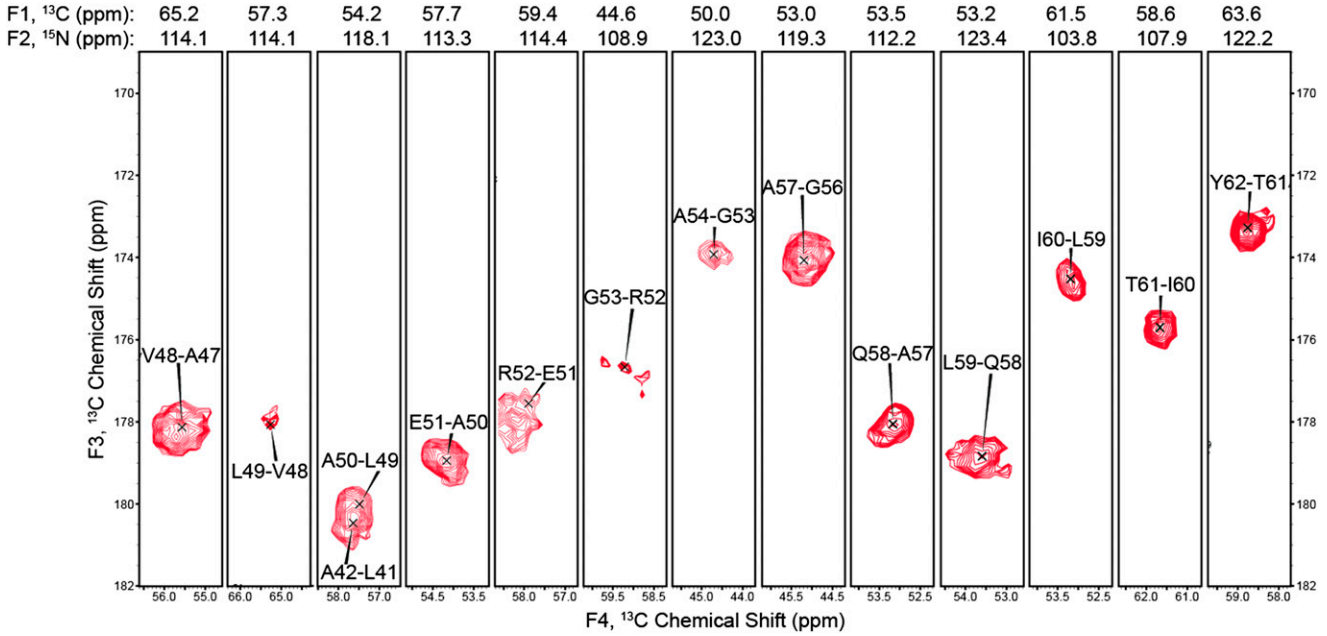

Fig. S2. CANCOCA (Cα-*N*-C′-Cα) backbone walk. The data presented are the backbone walk from the first extracellular loop of KcsA into the S1 helix. The spectra not only illustrate the utility of the CANCOCA experiment for assignments, but variations observed in line-widths and peak intensities report indirectly upon backbone motion and exchange. The slices corresponding to G56-P55 and P55-A54 are not provided because prolines were unlabeled in the sample of KcsA used for this experiment. The spectrum was acquired on a 600 MHz Infinity Plus SSNMR spectrometer (Agilent) and processed using 100 Hz of Gaussian apodization in all dimensions to maximize signal-to-noise in motionally broadened regions of the spectrum near G53 and L49. The G53-R52 and L49-V48 peaks appear narrower because the signal-to-noise threshold was held constant across all slices and they exhibited lower overall S/N (although significantly above the noise threshold). Full side-chain assignments for all resonance were then identified in 3D and 2D spectra.

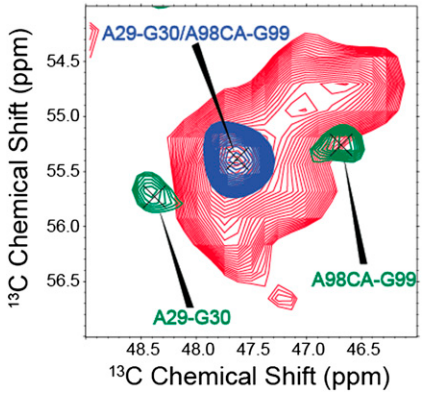

Fig. S3. Overlay of the G99-A98 Cα-Cα cross-peak as a function of [K^+] and pH. Spectra acquired at high [K^+]/pH conditions (blue) and low [K]/high pH conditions (green) are overlaid onto the high [K^+]/low pH spectrum. A majority of the marker peaks found to move under low [K^+] conditions are significantly broadened and difficult to observe at low pH. The G99 resonance is the main exception. This peak, although significantly broadened, is observable because the shift changes over the range of the structural ensemble encountered under low pH conditions. This observed structural heterogeneity suggests that although the gate structures of the low [K^+]/high pH and high [K^+]/low pH states are very similar, the hinge region of the protein exhibits greater conformational heterogeneity and dynamics compared with the low [K^+] state.

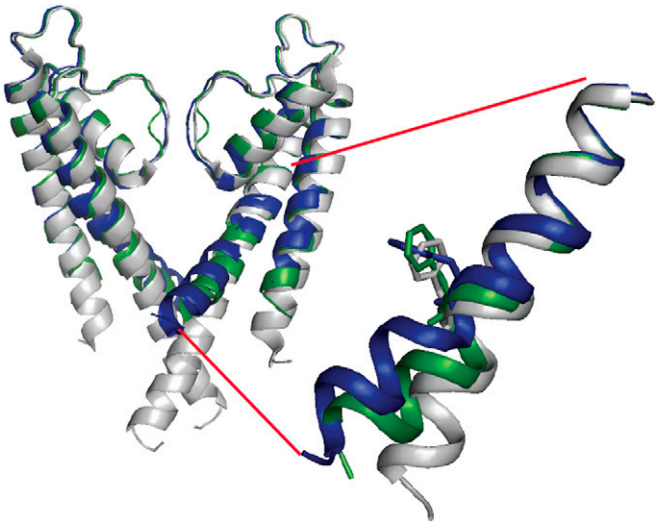

Fig. S4. Overlay of 3FB8 (green) and 3F5W (blue)[13] structures onto the 1K4D structure (gray). 3FB8 and 3F5W are structures of KcsA where a six-point mutation removes the interactions in the pH gate (H25Q, R117Q, E120Q, R121Q, R122Q, and H124Q), allowing channel opening under crystallographic conditions. Comparing these structures back to the 1K4D structure, it is observed that first, the 3F5W structure assumes the same nonconductive conformation of the selectivity filter observed in the low K^+ 1K4D structure despite being crystallized under high K^+ conditions. Both 3FB8 and 3FW5 exhibit kinks in the region from A98-G104. In the case of 3FB8, with only a 20 Å opening at T112 (compared with 12 Å resting distance and 32 Å distance in 3F5W), the largest perturbations in dihedral torsion angles are observed in the region from A98-T101, consistent with our measured chemical shifts. 3F5W, on the other hand, exhibits the greatest distortion of backbone dihedral degrees of freedom relative to 1K4D in the G104-F103 region. Our measured chemical shift perturbations are in greatest agreement with the 3FB8 structure, with the exception of a greater than expected deviation at S102, but largely consistent with an opening of 20 Å.

Table S1. Functionally characterized site-specific KcsA mutants that are altered in C-type inactivation rates

Residue	Location	Mutation	Effect of mutation
R64	Pore helix	R64A[14]	Suppresses inactivation
W67	Pore helix	W67F[15]	Suppresses inactivation
E71	Pore helix	E71A,[14] E71S,[16] E71H[16], etc.	Varied effects
Y82	Extracellular loop	Y82A[14]	Promotes inactivation
M96	TM2 near hinge	M96V,[17] M96C[17]	Promotes inactivation
F103	TM2 in hinge	F103A,[18] F103C[18]	Suppresses inactivation

The mutants are localized in three regions—the pore helix, the extracellular loop, and the hinge region of the channel.

Table S2. Agreement of measured chemical shifts at low [K^+] with chemical shifts predicted from X-ray crystal structures using SPARTA+ (1,2)

Structure	Resolution, Å	Opening, Å	$^{13}C\alpha$ rmsd, ppm	$^{13}C\alpha$ shift rmsd, hinge, ppm	Deviations in predicted $^{13}C\alpha$ shifts vs. 1K4D in hinge, ppm
1K4D	2.3	None	0.88	0.94	0
3FB5	2.8	14.5	1.03	1.04	0.15
3FB6	3.0	16	0.96	0.98	0.26
3F7Y	3.4	17	1.01	0.72	0.21
3FB8*	3.4	20	1.10	0.70	0.84
3F7V	3.2	23	1.18	1.09	1.78
3F5W	3.3	32	1.40	1.90	2.45
3PJS	3.9		2.04	2.34	2.09

Protons were added to each structure for prediction, using the Molprobity server (3, 4). Among these structures, only 1K4D is a structure solved at low [K^+]. Nevertheless, structures with openings greater than 20 Å have collapsed selectivity filter geometries consistent with the 1K4D structure (5). Structures 3FB5, 3FB6, 3FY7, 3FB8, 3F7V, 3F5W, and 3PJS are septuple mutants of KcsA (H25Q, L90C, R117Q, E120Q, R121Q, R122Q, and H124Q), where the pH gate has been mutated to allow channel opening under crystallographic conditions. All structures also contain *N*- and C-terminal deletions consistent with the 1K4D structure. The resolution of the structures is in the 3–4 Å range and typically lower for those with more open channels; the overall agreement of experimental shifts with back-predicted shifts degrades when the crystal structures upon which the predictions are based are poorly resolved. However, this is not the case in the hinge region, defined as residues 98–104. In this region, we observe an overall improvement as the channel opens to an aperture of 17–20 Å measured at residue T112. This suggests that our observed experimental shifts reflect upon a helical kink opened in this region of the protein, consistent with the predicted strong allosteric network coupling the two gates.

*Open and conductive in the presence of Rb^+.

1. Shen Y, Bax A (2007) Protein backbone chemical shifts predicted from searching a database for torsion angle and sequence homology. *J Biomol NMR* 38(4):289–302.
2. Shen Y, Bax A (2010) SPARTA+: A modest improvement in empirical NMR chemical shift prediction by means of an artificial neural network. *J Biomol NMR* 48(1):13–22.
3. Chen VB, et al. (2010) MolProbity: All-atom structure validation for macromolecular crystallography. *Acta Crystallogr D Biol Crystallogr* 66(Pt 1):12–21.
4. Davis IW, et al. (2007) MolProbity: All-atom contacts and structure validation for proteins and nucleic acids. *Nucleic Acids Res* 35(Web Server issue):W375–W383.
5. Cuello LG, Jogini V, Cortes DM, Perozo E (2010) Structural mechanism of C-type inactivation in K(+) channels. *Nature* 466(7303):203–208.

Table S3. Chemical shift markers for low [K^+] state

Residue	N	N	C′	C′	Cα	Cα	Cβ	Cβ	$C\gamma_1$	$C\gamma_1$	$C\gamma_2$	$C\gamma_2$	Cδ	Cδ
A29			180.3	*179.8*	55.4	*55.6*	18.4	*18.6*						
G30	105.4	*105.1*			47.8	*48.4*								
A31														
A32	116.4	*116.4*			55.4	*55.5*	16.4	*16.3*						
T33	112.3	*112.4*			67.5	*67.5*	68.1	*68.1*				*20.8*		
I38	116.6	*116.7*			66.1	*66.6*	37.8	*37.6*	29.3	*29.6*	17.3	*17.1*	14.1	*14.1*
V39	118.9	*117.4*												
A42			180.0	*179.6*	54.4	*54.4*	19.1	*19.2*						
G43	108.1	*107.1*												
S44	113.6	*113.6*			64.6	*64.6*	63.4	*63.4*						
V48	114.6	*114.9*			65.5	*65.4*	31.4	*31.4*						
L49	114.8	*115.1*												
A50					54.5	*54.4*								
E51	114.0	*113.8*			57.9	*57.8*	31.1	*31.1*	38.9	*38.5*			183.8	*183.8*
R52	114.8	*114.2*			59.1	*58.9*								
G53	108.9	*109.4*			44.8	*44.6*								
A54	123.2	*124.0*			50.2	*50.3*	18.4	*18.0*						
G56	111.0	*110.9*			44.9	*45.1*								
A57	119.9	*119.7*			53.5	*53.5*	21.4	*21.1*						
L59	124.2	*123.2*			53.3	*53.3*	39.5	*39.3*					25.1	*25.4*
I60	103.9	*103.8*			61.6	*61.7*	38.7	*38.5*	26.0	*26.2*	18.0	*18.5*	13.9	*13.6*
T61	108.4	*108.4*	173.3	*173.1*	58.9	*58.8*	72.0	*71.5*			22.8	*22.3*		
Y62	122.1	*122.1*	173.6	*173.6*	63.9	*63.9*	36.5	*36.6*						
R64	110.6	*110.4*			60.2	*60.2*	31.6	*31.3*						
W67					59.39	*59.0*	29.78	*30.3*	111.0	*109.7*				
W68					60.11	*59.7*	28.55	*28.8*	113.6	*113.4*				
S69	120.6	*123.0*			62.99	*63.3*	61.11	*60.7*						
V70	122.5	*122.8*			67.36	*66.4*	31.34	*31.6*	23.6	*23.6*	22.1	*22.0*		
E71	111.5	*108.6*			58.18	*58.7*	27.1	*26.8*	32.5	*31.0*			182.5	*180.3*
T72			174.6	*173.8*	66.97	*67.2*	68.1	*68.0*						
A73			176.4	*175.6*	55.16	*54.9*	19.02	*18.9*						
T74	97.21	*97.7*	176.2	*176.9*	61.1	*61.4*	69.72	*70.2*			21.53	*20.6*		
T75	108.9	*113.1*	172.6	*172.3*	63.15	*62.5*	69.28	*69.2*			21.67	*20.7*		
V76	119.9	*116.2*	178.9	*175.6*	66.23	*65.2*	31.82	*30.2*	23.2	*22.3*	20.3	*20.1*		
G77	99.12	*104.5*	174.5	*173.7*	48.69	*47.2*								
Y78	114.1	*116.4*	178.2	*178.0*	61.66	*57.3*	38.38	*37.4*						
G79	100.1	*99.9*			45.52	*46.3*								
D80	116.6	*114.2*	175.6	*175.7*	55.57	*54.8*	37.44	*37.0*	179.5	*179.0*				
L81	116.1	*117.3*			52.95	*53.4*	47.74	*48.5*	27.6	*27.0*				
Y82	113.8	*115.6*	172	*172.5*	55.5	*55.3*	34.89	*36.4*						
V84							32.57	*32.4*	21.3	*21.1*	18.3	*18.1*		
T85	115	*115.2*	174.6	*174.5*	60.69	*60.8*	72.47	*72.3*			22.9	*22.9*		
L86	121	*120.6*					41.31	*41.4*						
W87					59.31	*59.3*								
8G8	105.8	*105.0*												
9M6	114.9	*116.3*					33.71	*34.6*	33.0	*32.7*				
A98					55.52	*55.2*	18.43	*19.2*						
G99	105.9	*105.5*			47.75	*48.4*	—							
I100	119.8	*119.5*			66.12	*65.9*	38.9	*39.6*	26.0	*26.0*	18.3	*17.9*	14.3	*13.9*
T101	118.8	*118.0*					68.25	*68.3*						
S102	115.4	*117.2*			63.52	*63.2*	63.5	*64.4*						
F103	118.7	*117.3*			60.8	*60.0*	39.0	*37.3*						
G104	106.8	*106.0*												
T107					68.6	*68.5*								
A108	120.3	*120.3*												
A111					55.3	*55.5*	18.8	*18.9*						
T112	112.4	*110.8*			67.5	*67.6*	68.1	*68.2*						
W113	122.7	*121.8*												
V115					66.5	*67.0*								
G116	106	*105.8*												
E118					58.9	*59.7*	29.6	*29.8*	36.0	*34.8*			182.8	*177.4*
E120					59.2	*59.7*	28	*29.7*	36.2	*34.8*			182.7	*177.4*

Shifts listed in roman type indicate shift at 50 mM [K^+], and shifts given in italics are for the same site, but at 0.2 μM [K^+].